Tracking the Potential-controlled Synthesis of Cu-nanocuboids and Graphene-covered Cu-nanocuboids Under *Operando* CO_2 Electroreduction

Thanh Hai Phan§ [a], Karla Banjac§ [a], Fernando Cometto[a], Federico Dattila[b], Rodrigo García-Muelas[b], Núria López[b], and Magalí Lingenfelder*[a]

[a] Dr. T. H. Phan[§], K. Banjac[§], Dr. F. Cometto, Dr. M. Lingenfelder
Max Planck-EPFL Laboratory for Molecular Nanoscience and Technology
Ecole Polytechnique Fédérale de Lausanne (EPFL)
1015 Lausanne (Switzerland)
E-mail: magali.lingenfelder@epfl.ch

[b] F. Dattila, Dr. R. García-Muelas, Prof. Dr. N. López
Institute of Chemical Research of Catalonia (ICIQ), The Barcelona Institute of Science and Technology (BIST)
Av. Països Catalans 16, 43007 Tarragona (Spain)

[§] Shared authorship.

Abstract:

The electroreduction of CO_2 (CO_2RR) is a promising strategy towards sustainable fuels. Cu is the only earth-abundant catalyst capable of CO_2-to-hydrocarbons conversion; yet, its dynamic structure under *operando* CO_2RR conditions remains unknown. Here, we track the Cu structure *operando* by electrochemical scanning tunneling microscopy and Raman spectroscopy. Surprisingly, polycrystalline Cu surfaces reconstruct forming Cu nanocuboids whose size can be controlled by the polarization potential and the time employed in their *in-situ* synthesis, without the assistance of organic surfactants and-or halide anions. If the Cu-surface is covered by a graphene monolayer, smaller features with enhanced catalytic activity for CO_2RR can be prepared. The graphene protecting layer soften the 3D morphological changes that Cu-based catalysts suffer when exposed to aggressive electrochemical environments, and allows us to track the kinetic roughening process. This novel strategy is promising for improving Cu long-term stability and, consequently, controlling product selectivity.

The electrochemical reductive reaction responsible of the conversion of CO_2 (CO_2RR) into hydrocarbons is a highly promising solution for the production of renewable fuels.[1] One of the drawbacks of this technology is that most catalysts are not selective towards energy-rich C_{2+} fuels, and therefore their efficiency is limited. Cu is the only earth-abundant CO_2RR catalyst capable of converting CO_2 into hydrocarbons.[2–4] Initial optimization towards enhanced ethylene production relies on a morphology-selectivity relationship highlighting (100) facets[5,6] as ideal geometry for C-C coupling. This reflects in an outstanding interest in the synthesis of Cu nanocuboids (CuNCs) through colloidal chemistry[7], electrodeposition[8], electrochemical cycling[9], thermally-grown[10] or electrochemically-grown Cu oxides and halides.[11]

However, this morphology-selectivity trend based on post-mortem studies ignores the morphological evolution[12] of the catalysts during CO_2RR. Cu-based catalysts are highly dynamic: nanostructured electrocatalysts undergo fragmentation[13] and coarsening[14], while surface reconstructions[15–17] at the atomic scale occur on all Cu catalysts. These morphological changes greatly affect the catalysts' long-term stability (in terms of their catalytic activity and product selectivity).[18,19]. The goal of *operando* studies investigating surface dynamics is thus three-fold: first, to gain insight into the formation of CuNCs; second, to

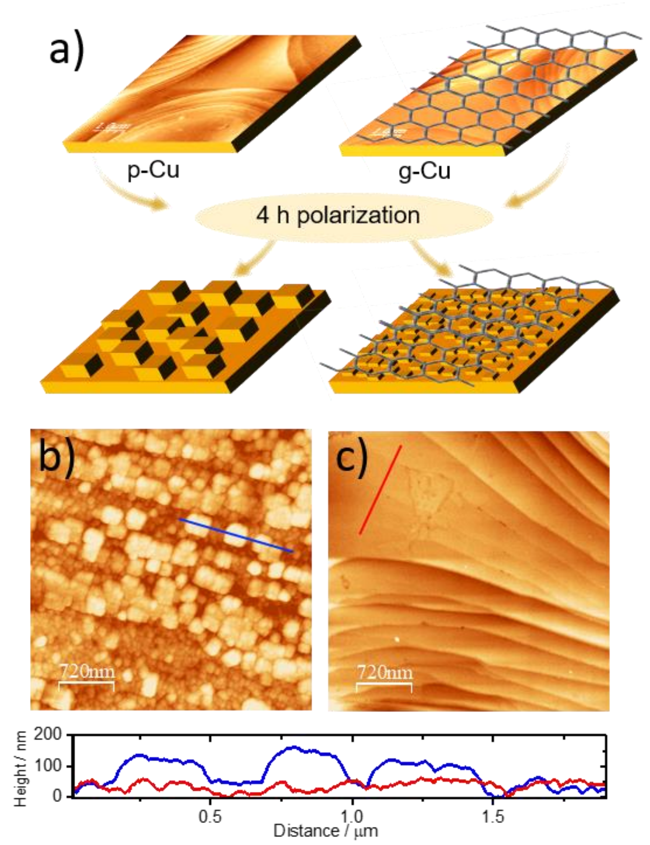

Figure 1. Scheme and *ex-situ* AFM images with corresponding height profiles showing the CuNCs formed on a-b) a pristine polycrystalline Cu-foil (p-Cu) and c) a graphene-covered (g-Cu) after polarization at -1 V *vs* Pt in a CO_2-saturated 0.1 M $KHCO_3$ solution for 4 hours.

correlate *operando* surface dynamics with the trends reported in product evolution over time; third, to explore possible strategies for morphology conservation by, for example, covering the catalyst surface with 2D materials.[20]

In this communication, we show the morphological transformation that polycrystalline Cu (p-Cu) and graphene-covered polycrystalline Cu (g-Cu) surfaces undergo after potentiostatic polarization at CO_2RR potentials over, at least, 4 hours. *In-situ* electrochemical scanning tunneling microscopy (EC-STM) experiments reveal the dynamics of the morphological evolution. Because Cu catalysts are highly prone to poisoning and deactivation during the first 30 minutes working at CO_2RR regimes, g-Cu represents an ideal substrate for these studies as graphene could act as a protective barrier.[21] Moreover, fresh g-Cu samples are oxide-free.[22] The thermal annealing of Cu foils under a reductive environment, performed as the pre-treatment step to CVD graphene growth, results in smooth surfaces[23], hence allowing high-resolution EC-STM imaging over an enlarged potential window.

CuNCs, reported earlier in the literature, were synthesized by electroreduction of Cu oxide or halide films, electrodeposition or by colloidal chemistry (protected by organic surfactants). To the best of our knowledge, this is the first report on CuNCs preparation by the one-step massive reconstruction of a Cu surface upon potentiostatic polarization in a halide-free electrolyte. Here, CuNCs growth during CO_2RR is related to a surface reconstruction mainly governed by the polarization of the substrate, in agreement with the reports on surface reconstructions of p-Cu to Cu(100).[15,17] In order to exclude the role of CO_2 on the mechanism of CuNCs formation, the same preparation protocol was conducted in a CO_2-free electrolyte, i.e. saturated with N_2: similar CuNCs were observed (Figure S2). This further supports a potential-driven surface reconstruction leading to CuNCs formation after prolonged exposure.

To gain knowledge on the surface reconstruction dynamics, we performed a series of *in-situ* EC-STM experiments to follow the transformation of the p-Cu surface underneath graphene. STM offers the unique possibility to monitor preferentially either the graphene layer or the Cu underneath by changing the STM bias conditions. The EC-polarization potential, located at a more negative value than the Cu_xO reduction potentials, is keep constant at the positive edge of CO_2RR and the hydrogen evolution reaction (HER) regime to avoid bubble evolution and interference of the Faradaic currents (crucial for *in-situ* EC-STM experiments). A dynamic observation of the different stages of the surface nanostructuration was followed by *in-situ* EC-STM on g-Cu (Figures 2a-g and S3). The initial stages of the surface reconstruction (Figures 2a-c) show how the polycrystalline Cu underneath the graphene is initially reconstructed to Cu mesocrystals within the first hour. Then, further reconstruction leads to nanometer-wide Cu(100) facets (Figures 2d-e). Figure 2e' shows that the graphene layer is still present during this reconstruction.

Small cuboid-features gradually grow on top of the Cu(100) facets; their size is gradually reducing as a function of time (as seen in Figures. 2f-g') reaching to an average edge length of ca. 4 ± 1 nm after 4 hours of polarization. The CuNCs size and the kinetics of formation can be tuned by changing the potentiostatic polarization time or applying more negative potential values (the more negative the potential value, the smaller the features and the shorter the times employed in the synthesis, Figure S4). DFT calculations proved that surface reconstruction is driven by surface polarization, see Supporting Discussion. Open facets such as Cu(100) store electrostatic energy more effectively than Cu(111) due to low coordination of surface Cu atoms (Figure S5-S6), therefore at very negative potentials they are more stable than closed-packed domains (Figure S7). By having a lower curvature, smaller structures experience a higher electric potential than flat surroundings, thus they undergo further reconstruction toward nanocuboid features with even lower Cu coordination.

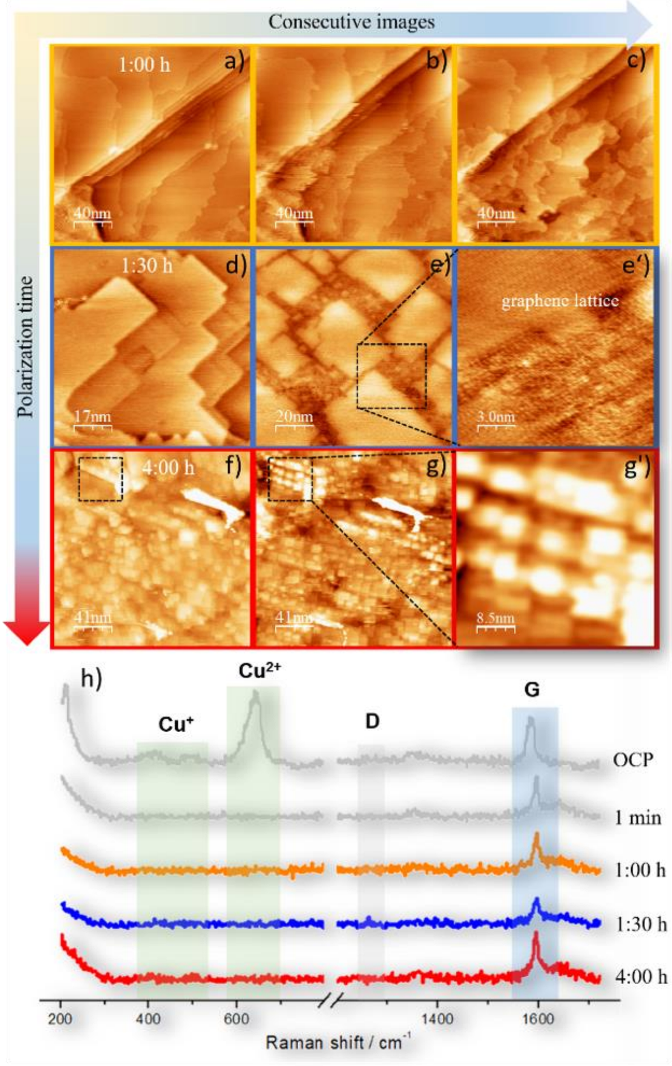

Figure 2. Series of EC-STM images showing the morphological evolution of a g-Cu surface upon polarization: a-c) from polycrystalline Cu to mesocrystals, d-e') to Cu(100) facets and f-g') to nanocuboids. E = -1.0 V vs Pt, U_b = 328 mV, I = 1.75 nA. h) *in-situ* Raman spectra showing the immediate reduction of native Cu_xO to metallic Cu and the presence of graphene during CuNCs formation on g-Cu.

Operando Raman spectra (Figure 2h) show the absence of native copper oxides during the morphological evolution. The peaks attributed to Cu_xO species[24,25] (≈410-500 cm^{-1} for Cu_2O and ≈621 cm^{-1} and CuO, respectively) disappear at the beginning of reconstruction, indicating that the native oxide layer present in air-exposed g-Cu surfaces was fully reduced.[26] This is in agreement with our EC-STM measurements showing smooth metallic Cu terraces (Figures 2a-g).

Interestingly, the graphene remains almost invariant on top of the as-prepared CuNCs. Figures 3a-b show *ex-situ* STM images of g-Cu surfaces before and after EC treatment, respectively. It can be observed that the hexagonal lattice of graphene is still present on top of the CuNCs. This suggests that the graphene layer remains intact during the *in-situ* synthesis of the NCs. The persistence of the graphene layer was also confirmed by both *operando* (Figure 2h) and *ex-situ* Raman spectroscopy (Figure 3c), where *ex-situ* spectra were collected on the same g-Cu sample before and after CuNCs formation. All spectra exhibit typical graphene peaks at ≈1591 cm^{-1} (the G band) and ≈2721 cm^{-1} (the 2D band).[27] The absence of the D-band (≈1350 cm^{-1}) on all spectra confirms the presence of a defect-free graphene layer before (i.e. on pristine g-Cu), during and after CuNCs formation. This further confirms that as-formed CuNCs are covered with graphene (g-CuNCs).

Following the same procedure, similar scenarios were observed on p-Cu. That is, initially polycrystalline Cu evolves gradually to mesocrystals, Cu(100) facets and cuboids (Figure S8). These results indicate that different Cu surfaces form nanocuboids after prolonged exposition to CO_2RR potentials (e.g. Cu foil, polished Cu, g-Cu, Cu functionalized with molecular additives[28] etc).

Even if the cuboid structures once formed conserve their morphology *ex-situ* at least for several days, a detailed analysis of the first steps in the formation of nanocuboid features points towards a kinetic roughening process, where multi-terrace islands (five-layered mounds, Figure S9) arise as a consequence of step-edge (Ehrlich-Schwoebel or ES) barriers[29,30] inhibiting downward transport of adatoms.

The fact that these are far-from-equilibrium structures is consistent with the sharp straight steps edges along [010] and [001] Cu(001) directions, in contrast to the edge-rounded equilibrium structures seen after homoepitaxy of Cu on Cu(001).[31,32] Moreover, the absence of fuzzy features points towards the absence of adsorbates at the Cu edges, again supporting a potential-driven roughening process. As the process happens also underneath graphene and at negative potentials, where no re-deposition of atoms is expected, the adatoms nucleating in the upper terraces might originate and diffuse from the grain boundaries. Further studies looking at the kinetics of the process under different electrolytes and pH conditions are underway, to asses if potential-driven reconstructions[33] as a kinetic phenomenon might be a general explanation for surface transformations observed on Cu and other metals during HER/CO_2RR.[34]

Finally, we performed a preliminary study comparing the CO_2RR/HER performance of the g-CuNCs to a Highly-Oriented Pyrolytic Graphite (HOPG) substrate (as a representative model system of the graphene layer) and to a pristine g-Cu sample. Linear sweep voltammograms corrected for electrochemically active surface area (ESCA) in a CO_2-saturated 0.1 M $KHCO_3$ are shown in Figure 3d. At negative potentials, cathodic current densities increase exponentially due to the CO_2RR and the parasitic HER. This effect is especially pronounced for g-CuNCs; where the presence of CuNCs underneath graphene leads to a shift in the HER/CO_2RR onset potentials to more positive values and increase the current density more than twice compared to the pristine g-Cu sample. These preliminary experiments hint that as-prepared g-CuNCs could show an enhanced HER/CO_2RR performance due to the unique combination of the (100) facets and confinement effects[35,36] at the Cu/graphene interface.

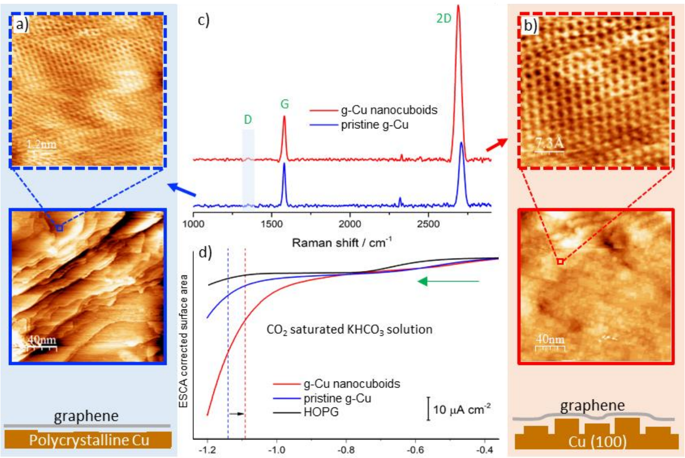

Figure 3. *Ex-situ* STM images showing graphene a) before and b) after reconstruction to g-CuNCs. U_b = 0.1 mV, I = 10.5 nA. c) *Ex-situ* Raman spectra of pristine g-Cu and g-CuNCs. Gray band highlights the wavenumber where the D band is usually observed. d) ESCA-corrected linear sweep voltammograms obtained for pristine g-Cu, g-CuNCs and HOPG.

In summary, we show that Cu surfaces suffer a drastic reconstruction under long exposure to negative potential values, evolving from polycrystalline Cu to nanocuboids, even in halide-free electrolytes. To prevent this massive reconstruction under *operando* conditions, we demonstrate the protective character of a single graphene layer on the Cu catalysts. The size of the nanocuboids can be tuned by the applied potential and/or the polarization time; e.g. 4 ± 1 nm g-CuNCs can be prepared after 4 h of polarization at -1 V vs Pt. A dynamic observation of the gradual surface reconstruction from polycrystalline Cu to nanocuboids is reported by *in-situ* EC-STM. As STM measurements cannot be performed in massively reconstructed Cu, this model system is ideal for *in-situ* studies. By both *operando* and *ex-situ* Raman spectroscopy, we show that the graphene layer on g-Cu remains intact during this process. This study opens new avenues to reinterpret the mechanism of nanostructured Cu-based materials without the presence of oxidized Cu species nor halides. In particular, it sheds light on the fact that Cu catalysts when normalized by the electrochemically active surface area (ECSA) show similar intrinsic activity[34]; most likely because the surface morphology (although highly dynamic) and step density under *operando* conditions are very similar at the atomic scale: the scale where ultimately CO_2RR occurs.

Acknowledgements

This work has received funding from the European Union’s Horizon 2020 research and innovation program under grant agreement No. 732840 A-LEAF. FD, RG-M and NL additionally acknowledge funding from European Union’s Horizon 2020 research and innovation program under grant agreement No. 722614 ELCOREL and from the Spanish Ministry of Science and Innovation (Grant RTI2018-101394-B-I00).

Keywords: CO_2 electroreduction • Copper electrocatalysis • *Operando* surface chemistry • Kinetic roughening • Graphene •

[1] X. Lim, *Nat. News* **2015**, *526*, 628.

[2] Y. Hori, A. Murata, R. Takahashi, S. Suzuki, *J. Chem. Soc. Chem. Commun.* **1988**, 17–19.

[3] A. A. Peterson, F. Abild-Pedersen, F. Studt, J. Rossmeisl, J. K. Nørskov, *Energy Environ. Sci.* **2010**, *3*, 1311–1315.

[4] K. P. Kuhl, E. R. Cave, D. N. Abram, T. F. Jaramillo, *Energy Environ. Sci.* **2012**, *5*, 7050–7059.

[5] Y. Hori, A. Murata, R. Takahashi, S. Suzuki, *J. Am. Chem. Soc.* **1987**, *109*, 5022–5023.

[6] A. Bagger, W. Ju, A. S. Varela, P. Strasser, J. Rossmeisl, *ACS Catal.* **2019**, *9*, 7894–7899.

[7] A. Loiudice, P. Lobaccaro, E. A. Kamali, T. Thao, B. H. Huang, J. W. Ager, R. Buonsanti, *Angew. Chem. Int. Ed.* **2016**, *55*, 5789–5792.

[8] Y. Wang, Z. Wang, C.-T. Dinh, J. Li, A. Ozden, M. Golam Kibria, A. Seifitokaldani, C.-S. Tan, C. M. Gabardo, M. Luo, H. Zhou, F. Li, Y. Lum, C. McCallum, Y. Xu, M. Liu, A. Proppe, A. Johnston, P. Todorovic, T.-T. Zhuang, D. Sinton, S. O. Kelley, E. H. Sargent, *Nat. Catal.* **2020**, *3*, 98–106.

[9] Y. Kwon, Y. Lum, E. L. Clark, J. W. Ager, A. T. Bell, *ChemElectroChem* **2016**, *3*, 1012–1019.

[10] R. Kas, R. Kortlever, H. Yılmaz, M. T. M. Koper, G. Mul, *ChemElectroChem* **2015**, *2*, 354–358.

[11] C. S. Chen, A. D. Handoko, J. H. Wan, L. Ma, D. Ren, B. S. Yeo, *Catal. Sci. Technol.* **2014**, *5*, 161–168.

[12] D. Kim, C. S. Kley, Y. Li, P. Yang, *Proc. Natl. Acad. Sci.* **2017**, *114*, 10560–10565.

[13] H. Jung, S. Y. Lee, C. W. Lee, M. K. Cho, D. H. Won, C. Kim, H.-S. Oh, B. K. Min, Y. J. Hwang, *J. Am. Chem. Soc.* **2019**, DOI 10.1021/jacs.8b11237.

[14] J. Huang, N. Hörmann, E. Oveisi, A. Loiudice, G. L. D. Gregorio, O. Andreussi, N. Marzari, R. Buonsanti, *Nat. Commun.* **2018**, *9*, 3117.

[15] Y.-G. Kim, J. H. Baricuatro, A. Javier, J. M. Gregoire, M. P. Soriaga, *Langmuir ACS J. Surf. Colloids* **2014**, *30*, 15053–15056.

[16] C. M. Gunathunge, X. Li, J. Li, R. P. Hicks, V. J. Ovalle, M. M. Waegele, *J. Phys. Chem. C* **2017**, *121*, 12337–12344.

[17] Y.-G. Kim, J. H. Baricuatro, M. P. Soriaga, *Electrocatalysis* **2018**, 1–5.

[18] P. Grosse, D. Gao, F. Scholten, I. Sinev, H. Mistry, B. Roldan Cuenya, *Angew. Chem. Int. Ed.* **n.d.**, *57*, 6192–6197.

[19] T. Möller, F. Scholten, T. N. Thanh, I. Sinev, J. Timoshenko, X. Wang, Z. Jovanov, M. Gliech, B. R. Cuenya, A. S. Varela, P. Strasser, *Angew. Chem. Int. Ed.* **2020**, *59*, 17974–17983.

[20] Y. Li, F. Cui, M. B. Ross, D. Kim, Y. Sun, P. Yang, *Nano Lett.* **2017**, *17*, 1312–1317.

[21] J. Hong, S. Lee, S. Lee, H. Han, C. Mahata, H.-W. Yeon, B. Koo, S.-I. Kim, T. Nam, K. Byun, B.-W. Min, Y.-W. Kim, H. Kim, Y.-C. Joo, T. Lee, *Nanoscale* **2014**, *6*, 7503–7511.

[22] S. Chen, L. Brown, M. Levendorf, W. Cai, S.-Y. Ju, J. Edgeworth, X. LI, C. W. Manguson, A. Velamakanni, R. D. Pinert, J. Kang, J. Park, R. S. Ruoff, *ACS Nano* **2011**, *5*, 1321–1327.

[23] S. M. Kim, A. Hsu, Y.-H. Lee, M. Dresselhaus, T. Palacios, K. K. Kim, J. Kong, *Nanotechnology* **2013**, *24*, 365602.

[24] X. Yin, Y. Li, F. Ke, C. Lin, H. Zhao, L. Gan, Z. Luo, R. Zhao, T. F. Heinz, Z. Hu, *Nano Res.* **2014**, *7*, 1613–1622.

[25] U. Lee, Y. Han, S. Lee, J. S. Kim, Y. H. Lee, U. J. Kim, H. Son, *ACS Nano* **2020**, *14*, 919–926.

[26] S. B. Scott, T. V. Hogg, A. T. Landers, T. Maagaard, E. Bertheussen, J. C. Lin, R. C. Davis, J. W. Beeman, D. Higgins, W. S. Drisdell, C. Hahn, A. Mehta, B. Seger, T. F. Jaramillo, I. Chorkendorff, *ACS Energy Lett.* **2019**, *4*, 803–804.

[27] S. D. Costa, A. Righi, C. Fantini, Y. Hao, C. Magnuson, L. Colombo, R. S. Ruoff, M. A. Pimenta, *Solid State Commun.* **2012**, *152*, 1317–1320.

[28] A. Thevenon, A. Rosas-Hernández, J. C. Peters, T. Agapie, *Angew. Chem. Int. Ed.* **2019**, *58*, 16952–16958.

[29] R. L. Schwoebel, E. J. Shipsey, *J. Appl. Phys.* **1966**, *37*, 3682–3686.

[30] G. Ehrlich, F. G. Hudda, *J. Chem. Phys.* **1966**, *44*, 1039–1049.

[31] J. C. Girard, Y. Samson, S. Gauthier, S. Roussel, J. Klein, *Surf. Sci.* **1994**, *302*, 73–80.

[32] J. B. Hannon, C. Klünker, M. Giesen, H. Ibach, N. C. Bartelt, J. C. Hamilton, *Phys. Rev. Lett.* **1997**, *79*, 2506–2509.

[33] A. S. Dakkouri, D. M. Kolb, in *Interfacial Electrochem. Theory Exp. Appl.* (Ed.: A. Wieckowski), Marcel Dekker Inc., New York, **1999**, pp. 151–173.

[34] S. Nitopi, E. Bertheussen, S. B. Scott, X. Liu, A. K. Engstfeld, S. Horch, B. Seger, I. E. L. Stephens, K. Chan, C. Hahn, J. K. Nørskov, T. F. Jaramillo, I. Chorkendorff, *Chem. Rev.* **2019**, DOI 10.1021/acs.chemrev.8b00705.

[35] H. Li, J. Xiao, Q. Fu, X. Bao, *Proc. Natl. Acad. Sci.* **2017**, *114*, 5930–5934.

[36] J. Wordsworth, T. M. Benedetti, A. Alinezhad, R. D. Tilley, M. A. Edwards, W. Schuhmann, J. Justin Gooding, *Chem. Sci.* **2020**, *11*, 1233–1240.